European Conference on Computational Fluid Dynamics
ECCOMAS CFD 2006
P. Wesseling, E. Oñate and J. Périaux (Eds)

ON THE USE OF SLOPE LIMITERS FOR THE DESIGN OF RECOVERY BASED ERROR INDICATORS

Matthias Möller[*], **Dmitri Kuzmin**[†]

[*]University of Dortmund, Institute of Applied Mathematics (LS III)
Vogelpothsweg 87, D-44227 Dortmund, Germany
e-mail: matthias.moeller@math.uni-dortmund.de
[†]University of Dortmund, Institute of Applied Mathematics (LS III)
Vogelpothsweg 87, D-44227 Dortmund, Germany
e-mail: kuzmin@math.uni-dortmund.de

Key words: gradient recovery, a posteriori error indicators, adaptive finite elements

Abstract. *Gradient recovery techniques for the design of* a posteriori *error indicators are reviewed in the context of fluid dynamic problems featuring shocks and discontinuities. An edgewise slope limiting approach*[24] *tailored to linear finite element discretizations is presented. The improved gradient values at edge midpoints are recovered as the limited average of constant slopes from adjacent triangles. Furthermore, the low-order gradients may serve as natural upper and lower bounds to be imposed on the edge slopes. To this end, approved techniques such as averaging projection*[33]*, the (superconvergent) Zienkiewicz-Zhu patch recovery (SPR*[34]*) and polynomial preserving recovery (PPR*[29]*) are used to predict high-order gradients. A slope limiter is applied edge-by-edge to correct the provisional edge gradient values subject to geometric constraints. In either case, a second order accurate quadrature rule is employed to measure the difference between consistent and reconstructed slopes in the (local) L_2-norm which provides a usable indicator for grid adaptation.*

The algebraic flux correction (AFC) methodology[14–19] *is equipped with adaptive mesh refinement/coarsening procedures governed by the recovery based error indicator. The adaptive algorithm is applied to inviscid compressible flows at high Mach numbers.*

1 INTRODUCTION

In a series of recent publications[14–19], an algebraic framework for the construction of high-resolution schemes for convection dominated partial differential equations was developed. The *algebraic flux correction* (AFC) paradigm renders a high-order discretization *local extremum diminishing* (LED) by a conservative elimination of negative off-diagonal entries from the discrete transport operator so as to end up with a non-oscillatory approximation of low order. In order to recover the high accuracy of the original, e.g., standard Galerkin scheme, compensating antidiffusion can be added whose magnitude must be modulated based on the local smoothness of the solution. To this end, the antidiffusive fluxes are limited by a nodal limiter of FCT or TVD type or by the recently proposed general-purpose limiter[14] which represents a combination thereof.

The adaptive blending of high- and low-order methods prevents us from using common error estimation approaches that require an *a priori* knowledge of the order of approximation, e.g., estimators for the truncation error[3,4] based on classical Richardson extrapolation. Gradient recovery techniques[33] seem to be a promising alternative, but their use in error estimation requires that the true solutions are sufficiently smooth.

This paper focuses on hyperbolic problems featuring shocks and discontinuities so that traditional recovery procedures may fail to be reliable. In what follows, limited averaging of consistent slopes is used to compute improved gradient values at midpoints of edges. As an alternative, classical recovery procedures are employed to predict provisional gradient values at edge midpoints which are corrected by means of a slope limiter. The upper and lower bounds to be imposed are given by the constant slopes of adjacent triangles.

2 A POSTERIORI ERROR INDICATORS

As a model problem, consider a generic partial differential equation $\mathcal{L}\mathrm{u} = f$ where the (possibly nonlinear) differential operator $\mathcal{L}$ may comprise both spatial and time derivatives. Its variational form is derived by integrating the weighted residual of the governing equation over the domain Ω and setting the result equal to zero

$$\int_\Omega w[\mathcal{L}\mathrm{u} - f]\,\mathrm{d}\mathbf{x} = 0. \tag{1}$$

Moreover, let the solution be approximated by means of finite elements

$$\mathrm{u} \approx u_h = \sum_j u_j \varphi_j, \tag{2}$$

where φ_j denote the basis functions spanning the finite-dimensional subspace $\mathcal{V}_h$. In this article, we shall concentrate on the numerical error resulting from the approximation of spatial derivatives and devise an *a posteriori* indicator for the vector-valued gradient error

$$\mathbf{e} = \nabla\mathrm{u} - \nabla u_h. \tag{3}$$

In this paper, the consistent gradient will also be referred to as low-order gradient

$$\nabla u_h = \sum_j u_j \nabla\varphi_j. \tag{4}$$

The basic idea of recovery based error estimators[33], is to replace the unknown values $\nabla\mathrm{u}$ of the exact slopes in equation (3) by a smoothed gradient field $\hat{\nabla} u_h$, so as to obtain

$$\mathbf{e} \approx \hat{\mathbf{e}} = \hat{\nabla} u_h - \nabla u_h \tag{5}$$

which may serve as a viable approximation to the true error defined in (3).

In general, pointwise error estimates are difficult to obtain, so integral measures are typically employed in the finite element framework. Let Ω_h denote a partition of the computational domain into a set of non-overlapping finite elements Ω_e so that the L_2-norm represents a usable measure for the error both globally and locally

$$||\hat{\mathbf{e}}||_{L_2}^2 = \sum_{\Omega_e} ||\hat{\mathbf{e}}||_{L_2(\Omega_e)}^2, \qquad ||\hat{\mathbf{e}}||_{L_2(\Omega_e)}^2 = \int_{\Omega_e} \hat{\mathbf{e}}^{\mathrm{T}}\hat{\mathbf{e}}\ \mathrm{d}\mathbf{x}. \tag{6}$$

In this paper, we only consider piecewise linear (P_1) finite elements on triangular meshes for which the consistent gradient $\nabla u_h = \left[\frac{\partial u_h}{\partial x_1}, \frac{\partial u_h}{\partial x_2}\right]$ is constant on each triangle. Hence, the improved slopes should be at least piecewise linear so as to provide a better approximation to the exact gradient. It suffices to specify slope values at all midpoints of edges, i.e., $\mathbf{x}_{ij} := \frac{1}{2}(\mathbf{x}_i + \mathbf{x}_j)$, to obtain a smoothed quantity $\hat{\nabla} u_h$ that varies linearly in each Ω_e and is allowed to exhibit jumps across inter-element boundaries. This approach can be seen as seeking the nodal values for a non-conforming approximation of $\hat{\nabla} u_h$ by means of linear Crouzeix-Raviart finite elements for which the local degrees of freedom are located at edge midpoints. For bilinear finite elements used on quadrilateral grids, a similar gradient approximation can be based on the non-conforming Rannacher-Turek element.

Let (6) be integrated via the second order accurate quadrature rule

$$\int_{\Omega_e} \hat{\mathbf{e}}^{\mathrm{T}}\hat{\mathbf{e}}\ \mathrm{d}\mathbf{x} = \frac{|\Omega_e|}{3} \sum_{ij} \hat{\mathbf{e}}_{ij}^{\mathrm{T}}\hat{\mathbf{e}}_{ij}, \qquad \text{where} \quad \hat{\mathbf{e}}_{ij} = \hat{\nabla} u_{ij} - \nabla u_{ij}. \tag{7}$$

In the above expression, $|\Omega_e|$ denotes the element area and all quantities are evaluated at the three midpoints of surrounding edges indicated by subscript ij. It remains to devise a procedure for constructing an improved gradient value $\hat{\nabla} u_{ij}$ for the edge $\vec{ij}$.

3 LIMITED GRADIENT AVERAGING

Our first approach to obtaining a smoothed edge gradient is largely inspired by slope limiting techniques employed in the context of high-resolution finite volume schemes and later carried over to discontinuous Galerkin finite element methods. For simplicity, let us illustrate the basic ideas for a one-dimensional finite volume discretization. The task is to define a suitable slope value u_j' on the interval $I_j = (x_{j-1/2}, x_{j+1/2})$ so as to recover a piecewise linear approximate solution from the mean value $\bar{u}_j$

$$u_h(x) = \bar{u}_j + u_j'(x - x_j), \qquad \forall\, x \in I_j. \tag{8}$$

In the simplest case, one-sided or centered slopes can be utilized to obtain first- and second-order accurate schemes which lead to rather diffusive profiles and are quite likely to produce non-physical oscillations in the vicinity of steep fronts and discontinuities, respectively. For a numerical scheme to be non-oscillatory, it should possess certain properties[16], e.g., be monotone, positivity preserving or total variation diminishing (TVD).

Jameson formulated a handy condition to show that a numerical scheme is local extremum diminishing[12] (LED), which represents a generalization of Harten's TVD theorem. In order to render a given approximation LED, he introduced a family of limited average operators[13] $\mathcal{L}(a,b)$ which are characterized by the following properties:

P1. $\mathcal{L}(a,b) = \mathcal{L}(b,a)$.

P2. $\mathcal{L}(ca,cb) = c\mathcal{L}(a,b)$.

P3. $\mathcal{L}(a,a) = a$.

P4. $\mathcal{L}(a,b) = 0$ if $ab \leq 0$.

While conditions P1–P3 are natural properties of an average, P4 is to be enforced by means of a limiter function. It has been demonstrated[13] that a variety of standard TVD limiters can be written in such form. Let the modified sign function be given by

$$\mathcal{S}(a,b) = \frac{\mathrm{sign}(a) + \mathrm{sign}(b)}{2} \tag{9}$$

which equals zero for $ab \leq 0$ and returns the common sign of a and b otherwise. Then the most widely used two parameter limiters for TVD schemes can be written as:

1. minmod: $\mathcal{L}(a,b) = \mathcal{S}(a,b)\ \min\{|a|,|b|\}$
2. maxmod: $\mathcal{L}(a,b) = \mathcal{S}(a,b)\ \max\{|a|,|b|\}$
3. Van Leer: $\mathcal{L}(a,b) = \mathcal{S}(a,b)\ \dfrac{2|a||b|}{|a|+|b|}$
4. MC: $\mathcal{L}(a,b) = \mathcal{S}(a,b)\ \min\left\{\dfrac{|a+b|}{2}, 2|a|, 2|b|\right\}$
5. superbee: $\mathcal{L}(a,b) = \mathcal{S}(a,b)\ \max\{\min\{2|a|,|b|\},\min\{|a|,2|b|\}\}$

Finally, the limited counterpart of u'_j in (8) can be computed as follows

$$\hat{u}'_j = \mathcal{L}\left(\frac{\bar{u}_{j-1} - \bar{u}_j}{\Delta x}, \frac{\bar{u}_{j+1} - \bar{u}_j}{\Delta x}\right). \tag{10}$$

Let us return to our original task that requires the reconstruction of smoothed solution gradients at edge midpoints. This is where the benefit of an edge based formulation comes into play. Except at the boundary, *exactly* two elements are adjacent to edge $\vec{ij}$ such that an improved gradient can be determined efficiently as the limited average of the constant slope values to the left and to the right by letting each component be defined as follows

$$\hat{\nabla} u_{ij} = \mathcal{L}(\nabla u_{ij}^{+}, \nabla u_{ij}^{-}). \tag{11}$$

It is easy to verify that for all limiter functions $\mathcal{L}$ presented above, the recovered edge gradient is *naturally* bounded from below and above by the constant slope values

$$\nabla u_{ij}^{\min} \leq \hat{\nabla} u_{ij} \leq \nabla u_{ij}^{\max}, \qquad \text{where} \qquad \nabla u_{ij}^{\substack{\max\\ \min}} = \max_{\min}\{\nabla u_{ij}^+, \nabla u_{ij}^-\}. \tag{12}$$

Note that the above inequality holds separately for each spatial component of the vector-valued gradient. Suppose the upper and lower bounds have different sign such that

$$\left[\frac{\partial u_{ij}^+}{\partial x_d}\right]\left[\frac{\partial u_{ij}^-}{\partial x_d}\right] < 0 \tag{13}$$

for, say, the d-th spatial component of the gradient. The mean value theorem states that its value is zero somewhere in-between. If this is true for all components of the gradient the approximate solution may attain a local extremum across the edge. Hence, property P4 of limited average operators acts as a discrete analog to the necessary condition for local extrema in the continuous case which requires the derivative to be zero.

To some extend, the recovered gradient (11) depends on the choice of the limiter $\mathcal{L}$. In the authors' experience, MC seems to be a safe choice as it tries to select the standard average whenever possible without violating the natural upper and lower bounds.

4 LIMITED GRADIENT RECONSTRUCTION

As an alternative to the limited averaging approach, traditional recovery procedures can be used to *predict* provisional gradient values at edge midpoints which are *corrected* by means of edgewise slope limiting so as to satisfy the geometric constraints set up by inequality (12). The idea of using recovery techniques to obtain improved gradient/stress values exhibits quite a long tradition in finite elements. In their first paper on recovery-based error estimation[33], Zienkiewicz and Zhu make use of so-called *averaging projection* schemes to construct smoothed slope values from the finite element solution as follows

$$\hat{\nabla} u_h = \sum_j \hat{\nabla} u_j \phi_j, \tag{14}$$

where the coefficients $\hat{\nabla} u_j$ are obtained by solving the discrete problem

$$\int_\Omega \phi_i(\hat{\nabla} u_h - \nabla u_h)\,\mathrm{d}\mathbf{x} = 0. \tag{15}$$

Note that the element shape functions used to construct the basis functions ϕ_j may be different those used in the finite element approximation (2). A detailed analysis[1] by Ainsworth *et al.* revealed the fact that the corresponding polynomial degrees should satisfy $\deg \phi \geq \deg \varphi$ whereby the original choice[33] $\phi = \varphi$ 'is not only effective, but also the most economical'[1] one. The substitution of equation (14) into (15) yields a linear algebraic system for each component of the smoothed gradient

$$M_C \hat{\nabla} u_h = \mathbf{C}\, u. \tag{16}$$

The consistent mass matrix $M_C = \{m_{ij}\}$ and the operator $\mathbf{C} = \{\mathbf{c}_{ij}\}$ which corresponds to the discretized spatial derivatives are assembled from the integral terms

$$m_{ij} = \int_\Omega \phi_i \phi_j \,\mathrm{d}\mathbf{x}, \qquad \mathbf{c}_{ij} = \int_\Omega \phi_i \nabla \varphi_j \,\mathrm{d}\mathbf{x}. \tag{17}$$

Note that the coefficients m_{ij} and $\mathbf{c}_{ij}$ remain unchanged as long as the mesh is kept fixed. As a consequence they need to be evaluated just once during the initialization step and each time the grid has been (locally) adapted. If $\phi \equiv \varphi$, the coefficients defined in (17) coincide with those required to assemble the finite element matrices and hence, are available at no additional costs. Moreover, the discrete operator $\mathbf{C}$ has zero row sums, i.e., $\sum_j \mathbf{c}_{ij} = 0$ as long as the sum of basis functions equals one at every point. This amenable feature allows for an efficient edge-by-edge assembly of the right-hand side

$$(\mathbf{C}\, u)_i = \sum_{j \neq i} \mathbf{c}_{ij}(u_j - u_i). \tag{18}$$

Interestingly enough, the system of algebraic equations (16) can also be obtained by applying the Galerkin approximation to the weak form of the continuous problem $\hat{\nabla} u = \nabla u$, where the weighting and basis functions may or may not be the same. Thus, projection schemes of the form (14)–(15) are called *variational recovery*[22] and can be applied repeatedly so as to determine an approximation to a higher-order derivative. In any case, the solution to (16) can be computed iteratively by successive approximation preconditioned by the lumped mass matrix $M_L = \mathrm{diag}\{m_i\}$, where $m_i = \sum_j m_{ij}$, as follows:

$$\hat{\nabla} u_h^{(m+1)} = \hat{\nabla} u_h^{(m)} + M_L^{-1}[\mathbf{C}\, u - M_C \hat{\nabla} u_h^{(m)}], \qquad m = 0, 1, 2, \ldots. \tag{19}$$

Mass lumping can also be applied directly to equation (16) which yields an explicit formula for computing the values of the projected gradient at each node

$$\hat{\nabla} u_i = \frac{1}{m_i} \sum_{j \neq i} \mathbf{c}_{ij}(u_j - u_i). \tag{20}$$

In general, provisional slopes at edge midpoints can be interpolated from the nodal values obtained either from (16) or (20) making use of representation (14). For linear finite elements this corresponds to taking the mean values for each edge $\vec{ij}$,

$$\hat{\nabla} u_{ij} = \hat{\nabla} u_h(\mathbf{x}_{ij}) := \frac{\hat{\nabla} u_i + \hat{\nabla} u_j}{2}. \tag{21}$$

It is also feasible to project the low-order gradient ∇u_h into the space of non-conforming (bi-)linear finite elements by letting $\phi_j \in \tilde{P}_1$ or $\tilde{Q}_1$ in equations (14)–(15), respectively. As a result, the smoothed slope values are directly available at the local degrees of freedom which, in this case, are located in the edge midpoints.

Over the years, a more accurate patch recovery technique (SPR) was introduced by Zienkiewicz and Zhu[34] which relies on the superconvergence property of the finite element solution at some exceptional, yet *a priori* known, points. Let the smoothed gradient be represented in terms of a polynomial expansion of the form

$$\hat{\nabla} u_h = p(\mathbf{x})\mathbf{a}, \tag{22}$$

where the row vector $p(\mathbf{x})$ contains all monomials of order k at most. Here, k denotes the degree of the finite element space, that is, $k = 1$ for (bi-)linear approximations. For each vertex, say i, there exists a patch Ω_i of elements surrounding this node. The multicomponent vector of coefficients $\mathbf{a} = [a_1, a_2, \dots, a_m]^{\mathrm{T}}$ in the above equation can be computed by means of a discrete least squares fit to the set of sampling points defined as

$$\mathcal{S}_i = \{ j \,:\, \mathbf{x}_j \in \Omega_i \} . \tag{23}$$

As a consequence, the quantity $\mathbf{a}$ can be determined by solving the linear system

$$M_p \, \mathbf{a} = \mathbf{f}, \tag{24}$$

where the local matrix M_p and the right-hand side vector $\mathbf{f}$ are given by

$$M_p = \sum_{j \in \mathcal{S}_i} p^{\mathrm{T}}(\mathbf{x}_j) \, p(\mathbf{x}_j), \qquad \mathbf{f} = \sum_{j \in \mathcal{S}_i} p^{\mathrm{T}}(\mathbf{x}_j) \, \nabla u_h(\mathbf{x}_j). \tag{25}$$

For system (24) to have a unique solution, its rank has to be at least equal to the number of terms in the polynomial expansion (22). In the two dimensional case this implies that $m \geq (k+1)(k+2)/2$. Hence, for linear ($k = 1$) finite elements, $p(\mathbf{x}) = [1, x, y]$ and the low-order gradient is sampled at the centroids of triangles which are known to exhibit optimal convergence rates. Except at the boundary, each node is surrounded by at least three elements, such that $m = 3$ holds for all interior vertices. For boundary nodes, Zienkiewicz and Zhu[34] suggest to evaluate their values from interior patches. However, it is easy to construct meshes for which two boundary components are only separated by one layer of elements such that no interior patches are available[20]. Moreover, the choice of the interior patch Ω_i may not be unique for unstructured triangulations[24].

Since the advent of the *superconvergent patch recovery* (SPR) technique[34] its super- and even ultraconvergence property has been analyzed extensively in the literature[28,31,32]. This paved the way for the development of so-called *polynomial preserving* (PPR) approaches[29]. While in SPR methods a polynomial of degree k is best fitted to the consistent gradient ∇u_h directly, PPR schemes determine a $k+1$ order accurate polynomial approximation to the finite element solution in the first place and apply the gradient operator afterwards. Recently, Zhang *et al.* introduced a 'meshless' gradient recovery method[30] in which the concept of element patches is abandoned in favor of spherical patches which can be expanded adaptively so as to guarantee the solvability of the local subproblems.

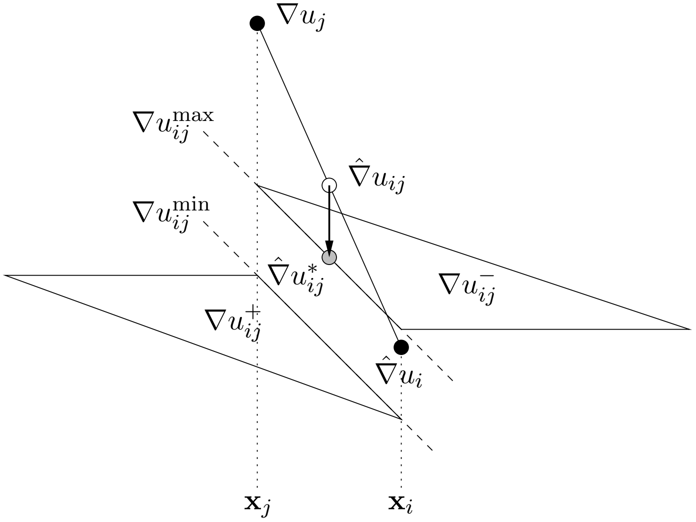

Figure 1: Edgewise slope-limited recovery.

The ease of implementation, generality and ability to produce quite accurate estimators boosted the popularity of recovery-based techniques especially in the engineering community. However, any of the above-mentioned strategies to predict the high-order gradient values may fail if the solution exhibits jumps or the gradient is too steep. This is typically the case for hyperbolic conservation laws such as the compressible Euler equations featuring strong shock waves. Recently, Korotov *et al.* demonstrated[10] that even for elliptic problems of the form $-\nabla \cdot (A\nabla u) = f$ standard gradient averaging may collapse if the coefficient matrix A is not smooth enough. This can be attributed to the fact that the averaging process extends over an *unsettled* number of surrounding element gradients which may strongly vary in magnitude and even possess different signs. Thus, it is very difficult the find admissible bounds to be imposed on such *nodal* gradients.

The transition to an edge based formulation makes it possible to correct the provisional slope values subject to their constant low-order counterparts, such that inequality (12) holds for each edge. It is also advisable to enforce the sign-preserving property (P4) of limited average operators so as to mimic the necessary condition of a local extremum in the discrete context. To this end, let $s_{ij} := \mathcal{S}(\nabla u_{ij}^{\min}, \nabla u_{ij}^{\max})$ for edge $\vec{ij}$, so that the corrected slope values $\hat{\nabla} u_{ij}^*$ can be computed from the predicted ones $\hat{\nabla}_{ij}$ as follows

$$\hat{\nabla} u_{ij}^* = s_{ij} \left| \max\{\nabla u_{ij}^{\min}, \min\{\hat{\nabla} u_{ij}, \nabla u_{ij}^{\max}\}\} \right| . \tag{26}$$

For an interior edge, the interplay of quantities involved in this predictor-corrector *edgewise limited recovery* (ELR) procedure are illustrated in Figure 1. The generality of this approach enables us to use arbitrary reconstruction techniques in the prediction step, e.g., L_2-projection, SPR and PPR schemes or the recent meshless variants[30] and apply edgewise slope-limiting as a black-box post-processing tool.

5 GRID ADAPTIVITY

In many CFD applications which can be modeled by hyperbolic conservation laws such as the compressible Euler equations of gas dynamics, the flow pattern is governed by the propagation and interaction of shock waves which dominate the error to a large extent. The occurrence of local phenomena suggests adaptive mesh refinement and coarsening as a useful tool for the cost-effective computation of highly resolved flow fields.

In adaptive solution procedures for steady state simulations, one typically starts with a moderately coarse grid on which an intermediate solution can be computed efficiently. Nevertheless, the mesh needs to be fine enough to capture all essential flow features in the solution and to enable the error indicator to detect 'imperfect' zones. If the artificial dissipation introduced by the numerical scheme overstrains the resolution facility of the underlying grid any error indicator can be misleading. This may explain the reported[25] failure of the Zienkiewicz-Zhu error estimator applied to shock wave computations.

Our simulation software is based on a geometric multigrid approach[6], for which the initial coarse grid is constructed by means of the advancing front algorithm implemented in the GiD mesh generator[8]. The hierarchical mesh data structure is assembled by successive subdivision of each element into four subtriangles. A common practice in compressible flow computations is to employ nested iterations[5,9] to speed up the convergence to steady state. In essence, a provisional solution is computed on a coarser mesh and interpolated to the next finer level so as to provide a reasonable initial guess.

The relative error of the density is used to monitor steady state convergence[7]. For intermediate solutions, the flow solver is stopped if the solution is halfway-converged[27], that is, if the relative error has reached the square root of the prescribed tolerance. The (more expensive) computation of a fully converged solution is performed on the final grid.

For a given (intermediate) solution, the grid is locally refined or coarsened according to some adaptation parameter and the whole process is repeated until (ideally) the global relative percentage error has dropped below the prescribed tolerance η_{tol}

$$\eta := \frac{||\mathbf{e}||_{L_2}}{||\nabla u||_{L_2}} \leq \eta_{\text{tol}}. \tag{27}$$

Since neither the exact slope values nor the true gradient error are known in the above equation, the best approximations available are utilized instead. From (6) it follows that the global L_2-norm can be decomposed into element contributions. Suppose the relative error is distributed equally between all cells Ω_e, then the above inequality holds provided the elementwise L_2-norm of the approximate gradient error satisfies

$$||\hat{\mathbf{e}}||_{L_2(\Omega_e)} \leq \eta_{\text{tol}} \left[\frac{||\nabla u_h||^2_{L_2} + ||\hat{\mathbf{e}}||^2_{L_2}}{|\Omega_h|} \right]^{1/2}. \tag{28}$$

Here, $|\Omega_h|$ stands for the total number of finite elements constituting the grid. Depending on the ratio of estimated and tolerated error, cells are marked for refinement or coarsening.

Once the new mesh has been constructed (see below), a usable initial guess $\tilde{u}_h$ is built from the old solution u_h. In general, global L_2-projection which is quite costly can be employed to transfer the solution between two arbitrary unstructured grids in a conservative fashion. If simpler interpolation techniques[21] or inaccurate quadrature are utilized, the loss of mass can be rectified by means of a mass restoration post-processing[11].

The alternating solution procedure and grid adaptation continues until some 'converged' mesh is obtained. To this end, either a maximum number of refinement levels is prescribed *a priori* or some more sophisticated stopping criteria may be devised. An economically cheap indicator can be based on the (relative) changes of the solution values on two successive grids and terminate the simulation if the difference is sufficiently small.

Grid refinement/coarsening techniques. The local grid refinement algorithm follows the regular *red-green* subdivision strategy[2] proposed by Bank *et al.* In a loop over elements, cells which are indicated for refinement are subdivided into four triangles. This so-called 'red' refinement is applied iteratively so as to eliminate adjacent cells with two or three hanging nodes. In order to restore global regularity of the triangulation the midpoints of bisected edges are connected to the opposite vertices. Prior to the next adaptation cycle, all edges which have been introduced due to this so-called 'green' refinement can/should be removed to retain the shape regularity of the successively refined grids.

As an alternative, conforming mesh refinement for triangular/tetrahedral grids can be accomplished by successive edge bisection[26]. For each element flagged for refinement, a new node is inserted at the midpoint of the longest edge and connected to the opposite vertex. The bisection process continues for all adjacent triangles sharing a hanging node with the refined element until all irregular grid points have been removed from the mesh. However, longest-edge bisection is mainly designed to uphold some *geometric* properties of the initial mesh and, thus, may not be the best comrade for our algebraic flux correction techniques[16–19]. For each element that needs to be refined due to accuracy reasons, the propagation path *solely* depends on the mesh geometry and does not account for the local solution behavior. In the framework of algebraic flux correction which entirely rests on an edge-based formulation, it is advisable to follow an *algebraic* edge partitioning approach. Recall that the amount of artificial dissipation that outlasts the flux limiter depends on the interplay of internodal fluxes which are proportional to the edgewise solution difference multiplied by some (anti-)diffusion coefficient. Therefore, it is quite expedient to bisect the edge with the largest solution variation or the largest antidiffusive flux[24].

If the relative gradient error (28) is sufficiently small for a patch of elements, a vertex removal procedure[11] is employed to coarsen the mesh. In essence, edge-swapping is performed repeatedly until the node is surrounded by just three triangles so that it can be safely removed. In case of a boundary node, an artificial element is introduced first to 'move' the vertex into the interior such that the standard procedure can be applied.

In the context of AFC schemes, edge collapsing may be a promising alternative. The basic idea is to contract edges and consolidate the two adjacent nodes whereby the position of the new vertex should improve the algebraic properties of the discretization[24].

6 NUMERICAL EXAMPLE

In order to illustrate the performance of the new algorithm let us consider a classical benchmark[27] problem for inviscid compressible flows which deals with multiple shock reflections. A supersonic flow at $M_\infty = 2$ enters a converging channel whose bottom wall is sloped at 5°. The initial triangulation was generated from a uniform mesh consisting of 60×16 quadrilaterals by dividing each element into two triangles. After three sweeps of local mesh refinement ($\eta_{\text{ref}} = 1\%$) and coarsening ($\eta_{\text{crs}} = 0.1\%$) governed by the MC-limited averaging error indicator, the zone of highest grid point concentration confines itself more and more to the vicinity of the shock as depicted in Figure 2. Moreover, the back and forth reflection of the shock leads to the separation of five zones of essentially uniform flow in which mesh coarsening takes place. Algebraic flux correction of TVD type[17] was employed to compute the solution, making use of the moderately diffusive CDS-limiter applied to the characteristic variables.

	exact	computed
ρ_I	1.000	1.000
ρ_{II}	1.216	1.216
ρ_{III}	1.463	1.462
ρ_{IV}	1.747	1.747
ρ_V	2.081	2.079
M_I	2.000	2.000
M_{II}	1.821	1.821
M_{III}	1.649	1.651
M_{IV}	1.478	1.479
M_V	1.302	1.304

Table 1: Converging channel: solution values.

The values of the normalized density distribution and the Mach number computed on the finest grid (15,664 elements) reveal an amazing agreement to the exact solutions for each of these subdomains as depicted in Table 1. The crisp resolution of the reflected shock wave can also be observed by considering the density 'cascade' drawn along the straight line $y = 0.6$ for all four grid levels. Interestingly enough, in the interior, the correct solution values are already obtained on the coarsest grid which may be attributed to the great resolution power of algebraic flux correction. However, the thin shock wave is smeared by excessive artificial diffusion that outlasts the flux limiting process which leads to underpredicted density values at the outflow boundary. This gap between the numerical solution at the boundary and the exact values as well as the steepness of the 'cascade' monotonically improves as the grid adaptation process continues.

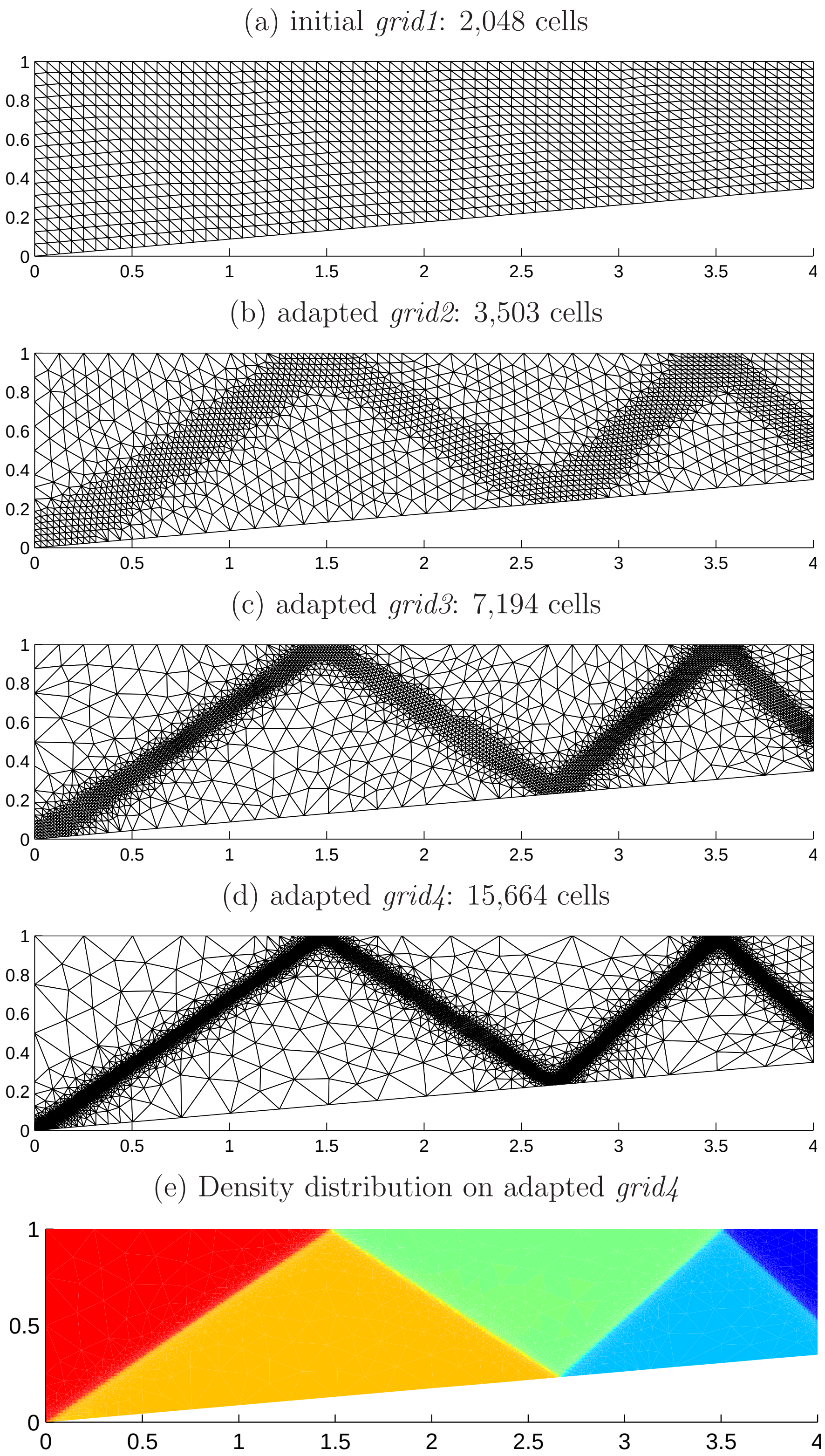

(a) initial *grid1*: 2,048 cells

(b) adapted *grid2*: 3,503 cells

(c) adapted *grid3*: 7,194 cells

(d) adapted *grid4*: 15,664 cells

(e) Density distribution on adapted *grid4*

Figure 2: Converging channel: grid adaptation.

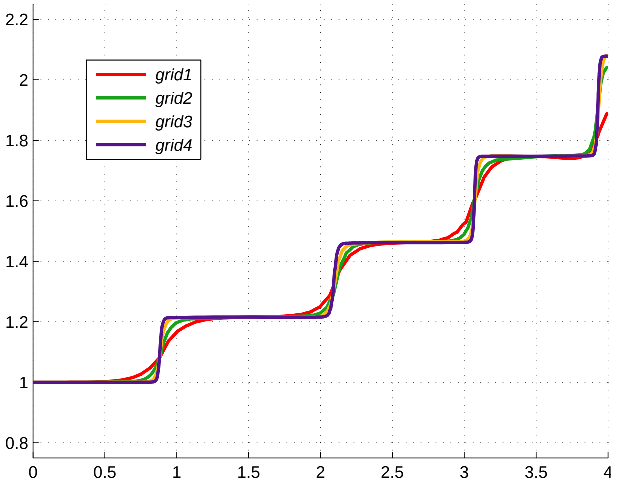

Figure 3: Converging channel: density cutlines at $y = 0.6$.

7 CONCLUSIONS AND OUTLOOK

The design of recovery-based *a posteriori* error indicators for hyperbolic conservation laws has been addressed. Slope limiting techniques provide a valuable tool for the construction of high-resolution gradient recovery procedures. Improved slopes can be directly computed at edge midpoints as a limited average of the constant gradients from adjacent triangles. These low-order slopes represent natural upper and lower bounds to be imposed on each edge gradient. Traditional (nodal) recovery procedures, e.g., Zienkiewicz-Zhu patch recovery or averaging projection schemes, can be used to predict high-order slopes which may violate the geometric constraints. As a remedy, a straightforward slope limiter is invoked edge-by-edge to correct the provisional gradient values.

The new error indicators were applied to algebraic flux correction[14–19] schemes which were successfully equipped with grid adaptivity. The highly unstructured meshes resulting from local mesh refinement/coarsening call for fully implicit discretizations which are unconditionally stable. The use of large (pseudo-)time steps which are especially amenable for the simulation of steady state flows comes at the cost of an increased effort required to solve the nonlinear equations. It could be worthwhile to employ a full approximation scheme (FAS) or devise a Newton[23] approach to tackle the strong nonlinearities.

REFERENCES

[1] M. Ainsworth, J.Z. Zhu, A.W. Craig, and O.C. Zienkiewicz. Analysis of the Zienkiewicz-Zhu a-posteriori error estimator in the finite element method. *Internat. J. Numer. Methods Engrg.*, 28(9):2161–2174, 1989.

[2] R.E. Bank, A.H. Sherman, and A. Weiser. Some refinement algorithms and data structures for regular local mesh refinement. In R. Stepleman, editor, *Scientific Computing, Applications of Mathematics and Computing to the Physical Sciences*, volume I of *IMACS Transactions on Scientific Computation*, pages 3–17. North-Holland, Amsterdam, 1983.

[3] M.J. Berger and P. Colella. Local adaptive mesh refinement for shock hydrodynamics. *J. Comput. Phys.*, 82(1):64–84, 1989.

[4] M.J. Berger and J. Oliger. Adaptive mesh refinement for hyperbolic partial differential equations. *J. Comput. Phys.*, 53(3):484–512, 1984.

[5] A. Brandt. Multi-level adaptive solutions to boundary value problems. *Math. Comp.*, 31(138):333–390, 1977.

[6] A. Brandt. Multi-level adaptive computations in fluid dynamics. *AIAA Journal*, 18(10):1165–1172, 1980.

[7] M. Feistauer, J. Felcman, and I. Straškraba. *Mathematical and Computational Methods for Compressible Flow.* Numerical Mathematics and Scientific Computation. Oxford University Press, 2003.

[8] Gid - the personal pre and postprocessor. `http://gid.cimne.upc.es/`.

[9] W. Hackbusch. *Iterative Solution of Large Sparse Systems of Equations*, volume 95 of *Applied Mathematical Sciences*. Springer, New-York, 1994.

[10] A. Hannukainen and S. Korotov. Computational technologies for reliable control of global and local errors for linear elliptic type boundary value problems. Technical Report A494, Helsinki University of Technology, 2006.

[11] P. Hansbo. A free-Lagrange finite element method using space-time elements. *Comput. Methods Appl. Mech. Engrg.*, 188(1–3):347–361, 2000.

[12] A. Jameson. Computational algorithms for aerodynamic analysis and design. *Appl. Numer. Math.*, 13(5):383–422, 1993.

[13] A. Jameson. Analysis and design of numerical schemes for gas dynamics 1. artificial diffusion, upwind biasing, limiters and their effect on accuracy and multigrid convergence. *Int. J. Comput. Fluid Dyn.*, 4:171–218, 1995.

[14] D. Kuzmin. On the design of general-purpose flux limiters for finite element schemes. I. scalar convection. Technical Report 299, University of Dortmund, 2005.

[15] D. Kuzmin and D. Kourounis. A semi-implicit FEM-FCT algorithm for efficient treatment of time-dependent problems. Technical Report 302, University of Dortmund, 2005.

[16] D. Kuzmin and M. Möller. Algebraic flux correction I. scalar conservation laws. In D. Kuzmin, R. Löhner, and S. Turek, editors, *Flux-Corrected Transport, Principles, Algorithms, and Applications*, pages 155–206. Springer, Germany, 2005.

[17] D. Kuzmin and M. Möller. Algebraic flux correction II. compressible Euler equations. In D. Kuzmin, R. Löhner, and S. Turek, editors, *Flux-Corrected Transport, Principles, Algorithms, and Applications*, pages 207–250. Springer, Germany, 2005.

[18] D. Kuzmin, M. Möller, and S. Turek. Multidimensional FEM-FCT schemes for arbitrary time-stepping. *Internat. J. Numer. Methods Fluids*, 42(3):265–295, 2003.

[19] D. Kuzmin and S. Turek. Flux correction tools for finite elements. *J. Comput. Phys.*, 175(2):525–558, 2002.

[20] P. Labbé and A. Garon. A robust implementation of Zienkiewicz and Zhu's local patch recovery method. *Comm. Numer. Methods Engrg.*, 11:427–434, 1995.

[21] R. Löhner. Robust vectorized search algorithms for interpolation on unstructured grids. *J. Comput. Phys.*, 118:380–387, 1996.

[22] P.R.M. Lyra. *Unstructured Grid Adaptive Algorithms for Fluid Dynamics and Heat Conduction*. PhD thesis, University of Wales, Swansea, 1994.

[23] M. Möller. Efficient solution techniques for implicit flux limiting finite element schemes. In preparation.

[24] M. Möller and D. Kuzmin. Adaptive mesh refinement for high-resolution finite element schemes. Technical Report 297, University of Dortmund, 2005.

[25] S. Prudhomme. Adaptive finite element simulation of a supersonic underexpanded jet. Master's thesis, University of Virginia, 1992.

[26] M.C. Rivara. Design and data structure of fully adaptive, multigrid, finite-element software. *ACM Trans. Math. Software*, 10(3):242–264, 1984.

[27] R.A. Shapiro. *Adaptive Finite Element Solution Algorithm for the Euler Equations*, volume 32 of *Notes on Numerical Fluid Mechanics.* Vieweg, Braunschweig-Wiesbaden, 1991.

[28] Z. Zhang. Ultraconvergence of the patch recovery technique II. *Math. Comp.*, 69:141–158, 2000.

[29] Z. Zhang and A. Naga. A posteriori error estimates based on polynomial preserving recovery. *SIAM J. Numer. Anal.*, 42(4):1780–1800, 2004.

[30] Z. Zhang and A. Naga. A new finite element gradient recovery method: Superconvergence property. *SIAM J. Sci. Comput.*, 26(4):1192–1213, 2005.

[31] Z. Zhang and J.Z. Zhu. Analysis of the superconvergent patch recovery technique and a posteriori error estimator in the finite element method (I). *Comput. Methods Appl. Mech. Engrg.*, 123(1–4):173–187, 1995.

[32] Z. Zhang and J.Z. Zhu. Analysis of the superconvergent patch recovery technique and a posteriori error estimator in the finite element method (II). *Comput. Methods Appl. Mech. Engrg.*, 163(1–4):159–170, 1998.

[33] O.C. Zienkiewicz and J.Z. Zhu. A simple error estimator and adaptive procedure for practical engineering analysis. *Internat. J. Numer. Methods Engrg.*, 24(2):337–357, 1987.

[34] O.C. Zienkiewicz and J.Z. Zhu. The superconvergent patch recovery and a posteriori error estimates. Part 1: The recovery techniques. *Internat. J. Numer. Methods Engrg.*, 33(7):1331–1364, 1992.